Journal of Materials Chemistry A

Accepted Manuscript

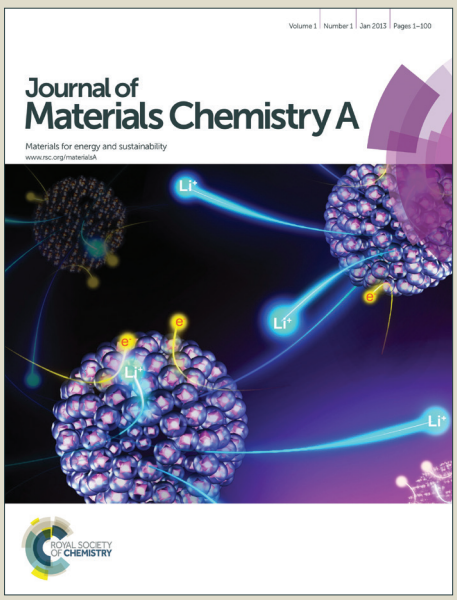

ROYAL SOCIETY OF CHEMISTRY

www.rsc.org/materialsA

Journal of Materials Chemistry A

ARTICLE

Pt/Porous Nanorods of Ceria as Efficient High Temperature Catalysts with Remarkable Catalytic Stability for Carbon Dioxide Reforming of Methane

Received 00th January 20xx,
Accepted 00th January 20xx

DOI: 10.1039/x0xx00000x

www.rsc.org/

Zhiyun Zhang [a], Jing Li [a], Wei Gao[a], Yuanyuan Ma [a]*, Yongquan Qu [ab]*

Porous nanorods of ceria (*PN*-Ceria) with a large oxygen storage capacity and a high concentration of oxygen vacancies exhibited better thermal stability compared to other nanocerias. No obvious structural deconstruction of *PN*-Ceria was observed when the material was annealed at 800°C. As the support of metal nanocatalysts, Pt exhibited a high dispersion on *PN*-Ceria and presented a high activity and catalytic stability for carbon dioxide reforming of methane (CRM) reaction at a high temperature of 800 °C. Catalytic activity of Pt/*PN*-Ceria catalysts in terms of methane conversion was only slightly decreased from 77.3 % to 74.2 % with a slow carbon deposition of 0.1 mg coke · g_{cat}^{-1} · h^{-1} after 72 hours CRM reaction at 800 °C. In contrast, a large decay in methane conversion (16.2 %) was observed for Pt/nonporous nanorods of ceria at the same reaction conditions. The high and robust catalytic activity of Pt/*PN*-Ceria catalysts can be ascribed to the unique physicochemical properties of *PN*-Ceria by preventing the sintering of Pt nanocatalysts into big particles and the formation of coke at rigid reaction conditions. Hence, more accessible active sites of Pt/*PN*-Ceria catalysts are provided for the CRM. Besides, the high concentration of oxygen vacancy and fast mobility of lattice oxygen of *PN*-Ceria also benefited the catalytic activity, stability and anti-coke deposition.

Introduction

Carbon dioxide and methane are two of the most abundant greenhouse gases contributing to the global climate change. Recently, controllable release and efficient utilization of the carbon dioxide and methane have been given extensive attention.[1, 2] Carbon dioxide reforming of methane(CRM) is considered as one of the most effective processes that simultaneously convert two greenhouse gases into hydrogen and carbon monoxide (known as synthesis gas, syngas).[3-5] Syngas can be used as fuel or an intermediate in many industrial processes for chemical synthesis. The optimal ratio ~ 1 of hydrogen to carbon monoxide in CRM reaction is more desirable for downstream synthesis to transform syngas into valuable chemicals through the subsequent reactions, such as Fisher-Tropsch reactions and oxosynthesis.[6-9]

Due to the strongly endothermic feature of the CRM reaction ($CH_4 + CO_2 \rightarrow 2CO + 2H_2$, $\triangle H_{298}$ = 247 kJ/mol), the reaction occurs at the elevated temperature in the range of 500 ~ 900 °C, which is required to reach high conversion levels of the reactants.[10-12] Various catalysts have been investigated for CRM, including mono- or bimetallic clusters on various supports.[8, 13-16] However, such severe operating temperatures result in a serious catalytic deactivation by sintering of both metallic catalysts and supports. Another problem is the carbon deposition on the surface of catalysts. CO disproportionation reaction ($2CO \rightarrow CO_2 + C$, $\triangle H_{298}$ = - 172 kJ/mol), an exothermic reaction, prefers to happen at lower temperatures. While, methane decomposition ($CH_4 \rightarrow C + 2H_2$, $\triangle H_{298}$ = 75 kJ/mol), an endothermic reaction, can occur at higher temperatures.[10] In either case, carbon deposition on the surface of the catalysts can happen and practically destroy the catalytic activity.[6, 17] Thus, it is extremely expected to develop effective CRM catalysts exhibiting high catalytic activity and selectivity as well as good stability.

[a] Centerfor Applied Chemical Research, Frontier Institute of Science and Technology, and State Key Laboratory for Mechanical Behavior of Materails, Xi'an Jiaotong University, Xi'an, China, 710049.E-mail: yongquan@mail.xjtu.edu.cn; yyma@mail.xjtu.edu.cn. Tel: +86-29-83395357.
[b] MOE Key Laboratory for Nonequilibrium Synthesis and Modulation of Condensed Matter, Xi'an Jiaotong University, Xi'an, China 710049

† Footnotes relating to the title and/or authors should appear here.
Electronic Supplementary Information (ESI) available: [The synthesis procedure of CeO_2 nanostructures, characterization, and the thermal stability evaluation characterized. The XRD patterns and XPS spectra of the Pt 4f for Pt/CeO_2]. See DOI: 10.1039/x0xx00000x

An ideal CRM catalyst is usually comprised of two closely integrated elements: a catalytic active metallic component for CRM reaction and a support to facilitate the desired reactions, immobilize the active centers, and maintain the metal dispersion of the catalyst under the high temperature. Meanwhile, catalysts have to be resistant to carbon deposition at the high temperatures.[7, 8, 18, 19] The additives are also introduced to accelerate the CRM reaction and stabilize the catalysts at high temperatures if necessary.[15, 20] However, to design catalysts suitable for high temperature CRM reaction in the complicated reactive environments is a daunting task.

It is well known that the melting point of the small metallic catalysts is significantly reduced due to the quantum confinement effect compared to their bulk counterpart, leading to a serious sintering and agglomeration of metallic nanoparticles on supports for CRM reaction at high temperatures.[21, 22] Several methods have been developed to counter this problem. For example, metal catalysts can be deposited on the pores of mesoporous alumina that can help retain the size of catalysts.[7, 23] Solid solutions(NiMgO et.al.) have been found to be quite robust, although only a small percentage of the catalysts are on the surface of solid solution substrates.[4] In addition, it has been shown that small metal catalysts (<6 nm) can effectively resist carbon deposition, significantly better than the larger ones.[24-26] Hence, the supports with the a strong interaction between metallic catalysts to maintain the small size of the metal catalysts and a remarkable anti-coke formation ability are of great importance on the catalytic activity and stability of the catalysts.[27]

Normally, large surface areas of supports are needed to host a large amount of small metallic catalysts.[21] However, most of the highly porous support frameworks are fragile at the high temperatures. For example, although porous Al_2O_3 displays much better thermal stability at the high temperature, the morphological change such as pore collapse has been observed after CRM reaction.[28] This would result in the closure of the pores and denying the accessibility of the reactants to the catalysts deposited within the pores. Pioneer studies have indicated that the addition of basic promoters into the framework of the supports not only has the potential to enhance their thermal stability but also can stabilize the metal catalysts at the high temperatures.[7] Incorporation of Zr into SiO_2 and Al_2O_3 significantly promoted the metal dispersion and their long-term stability for CRM.[20, 28] MgO is another example of promoter to suppress the sintering of Ni species on supports through the formation of NiO-MgO solid solution.[4, 29, 30] Furthermore, introducing basic promoters also enhances the catalytic activity and decreases the coke formation rate. The presence of Lewis basic sites in the catalysts can promote chemisorption of the CO_2 during the CRM reaction and accelerate the elimination of coke through the reaction between CO_2 and amorphous carbon to release CO.[6, 31]

Among various Lewis basic promoters, CeO_2, with the reversible transformation between Ce^{3+} and Ce^{4+}, shows excellent capacity to stabilize the metal nanocatalysts resulted from the strong metal-support interaction (SMSI) and effective ability to resist the coke formation originated from high oxygen mobility of CeO_2 itself. Thus, it has been widely used as the effective promoter into the frameworks of mesoporous Al_2O_3 and SiO_2 as the catalysts for CRM reaction.[7, 21, 23] Recently, metal nanocatalysts loaded on pure CeO_2 have been widely studied with the expectation of high catalytic activity and stability for CRM reaction.[8, 14, 18] However, the stable activity with time on stream (TOS) of metal/CeO_2 catalysts for CRM reaction has not been achieved. The major reason for the degraded activity is attributed to the significantly decreased oxygen storage capacity of CeO_2 due to its low thermal stability under the reductive atmosphere of CRM reaction.[32] The coke formation and the sintering of metal nanoparticles are generally observed in the catalysts using CeO_2 as supports after reaction, despite of the merits of CeO_2 as the supports for CRM reaction.

Recently, our group developed a novel synthetic route to produce a previously unknown CeO_2 nanostructure—porous nanorods of CeO_2 (*PN*-Ceria), which displayed a very large surface area and an extremely large oxygen storage capacity up to ~ 900 μmol O_2/g.[33] In this work, we demonstrate that porous CeO_2 nanorods exhibit good thermal stability at high temperatures, which can provide more accessible surface catalytic sites under the high operation temperatures. Combining their intrinsic physiochemical properties, the high catalytic activity and the long-term stability of Pt/*PN*-Ceria catalysts have been verified for CRM reaction in this work. Characterizations of Pt/*PN*-Ceria catalysts after 72 hours CRM reaction indicate that the catalysts maintain the highly dispersed Pt nanoparticles and effectively suppress the carbon deposition.

Experimental Section

All reagents were analytical grade and used without further purification. Thermal stability of nanocerias was evaluated for nanoparticles (in supporting information), porous nanorods, and nonporous nanorods, which were synthesized according to previously reported methods[34-36] and our previous study.[33]

Synthesis of Nonporous CeO_2 Nanorods (*NR*-Ceria)

1.736 g of $Ce(NO_3)_3{\cdot}6H_2O$ was dissolved in 10 mL of MQ water, and 19.2 g of NaOH was dissolved in 70 mL of MQ water. After aging of the mixed solution of $Ce(NO_3)_3{\cdot}6H_2O$ and NaOH for 30 min at room temperature, the mixture was transferred into a stainless steel autoclave for hydrothermal treatment at 100 °C for 24 h. The pressure of the autoclave was ~ 3.0 atm. The products were centrifuged off, washed by copies amount of MQ water, and dried at 60 °C overnight.

Synthesis of *PN*-Ceria

$Ce(NO_3)_3{\cdot}6H_2O$ (1.736 g) and NaOH (19.2 g) were dissolved in 10 and 70 mL of MQ water, respectively. The two solutions were thoroughly mixed in a Pyrex bottle and the mixture was aged under continuous stirring for 30 min at room temperature. Subsequently, the mixture was transferred into a temperature-controlled electric oven at 100 °C for 24 h. The internal pressure was controlled at ~ 1.2 atm by sealing the reaction vessel. After cooling down naturally, the bright yellowish products, nonporous $Ce(OH)_3/CeO_2$ nanorods, were collected by centrifugation and washing with MQ water and ethanol for three times. Of note, the lower pressure of the reaction

vessel is very critical to form the nonporous $Ce(OH)_3/CeO_2$ nanorods. Finally, the nonporous $Ce(OH)_3/CeO_2$ nanorods precursor were dried at 60 °C overnight. The *PN*-Ceria was synthesized by a continuous hydrothermal treatment of the nonporous nanorod precursor dispersion (2 mg/ml in water) at 160 °C for 12 h. The yellowish products were collected by centrifugation, washing and drying at 60 °C overnight. The synthetic details can be found in our previous reports.[33]

Synthesis of Pt/CeO_2 Catalysts

Pt catalysts supported on the *PN*-Ceria and *NR*-Ceria were prepared by wet impregnation method.[15] Briefly, the supports were dispersed in a solution of $H_2PtCl_6 \cdot 6H_2O$ in ethanol at room temperature. After continuous stirring at room temperature for 6 h and ethanol evaporation at 60 °C, the solids were dried and calcined at 100 °C and 500 °C for 8 and 4 h, respectively. The Pt loading percentage (0.57 wt%) was controlled by the added amount of the nanoceria supports and Pt salt.

Characterization

Transmission electron microscopy (TEM) was conducted on a Hitachi HT7700 microscopy at an accelerating voltage of 120 kV. Powder X-ray diffraction (XRD) data were collected using a PW 1710 Philips Powder X-ray diffractometer. X-ray photoelectron spectra (XPS) of freshly H_2-reduced (in situ at 623 K) catalysts were acquired on a Thermo Electron Model K-Alpha with Al Kα as the excitation source. The Pt content was determined by inductively coupled plasma optical emission spectroscopy (ICP-OES) analysis (Agilent 7500ce). Nitrogen adsorption and desorption measurements were performed on an ASAP 2020 HD88 (Micromeritics, Co). The samples were degassed at 80 °C under vacuum to ensure a clean dry surface. The specific surface area was calculated by the Brunauer-Emmett-Teller (BET) method and the pore size distribution was measured from the desorption branch of isotherms using the Barrett-Joyner-Halenda (BJH) method.

H_2 temperature-programmed reduction (H_2-TPR) was carried out in a ChemBET TPR/TPD3000 apparatus. In each run, 100 mg of catalyst was pretreated at 300°C for 30 min in a flowing stream of high-purity argon (30 mL·min^{-1}). After cooling to room temperature, a 10 % H_2 in Ar with a flow rate of 30 mL·min^{-1} was introduced and the programming temperature was controlled from room temperature to 900°C with a ramping rate of 10°C/min.

The dispersion of Pt was calculated from CO chemisorption by using pulses of a gas mixture containing 10 % CO in He at room temperature. The sample (200 mg) was reduced at 350 °C for 1 h in H_2 flow (10 mL·min^{-1}), then cooled down to 20 °C and purged with He (30 mL·min^{-1}) for 20 min. A given amount of CO (50 μL) was introduced in a pulse per 5 min until the intensity of the peak reached a constant value.

TGA-DSC (Thermogravimetry-Differential Scanning Calorimetry) analysis with a Netzsch STA449C thermoanalyzer was also used to determinethe amount of carbon deposited for the used catalysts. The sample was placed in a platinum crucible using an empty platinum crucible as a reference. The temperature was raised from room temperature to 800 °C at a rate of 10 °C /min in air.

Catalytic Reaction

The catalytic activity (90mg of catalyst) was measured in a fixed-bed quartz reactor (with an inner diameter of 0.3 cm and a length of 30 cm) at atmospheric pressure connected to a flow apparatus equipped with mass flow controllers. The catalysts were reduced in a 5% H_2 (99.995%)/Ar (99.999%) mixture (100 mL·min^{-1}) at 350 °C and isothermally kept at this temperature for 4 h. The dry reforming of methane was studied with a mixture of CH_4 (99.99%): CO_2 (99.99%): Ar (9: 9: 45 volume ratio) and a total GHSW of 30,000 mL·g^{-1}·h^{-1}. The measurements of the catalytic activity were carried out from 500 °C to 800 °C with a ramping rate of 5 °C/min. The effluent product gases were analyzed by online GC equipped (GC-1690, JieDao Tech) with TCD (thermal conductive detector, using TDX-01 column and 5A molecular sieve column) and FID (flame ionization detector, using a Porapark-Q column). Long-term stability of catalysts was carried out at 800 °C for 72 h. The catalytic properties were evaluated in terms of CH_4 and CO_2 conversions and H_2/CO ratio as follows:[37]

$$CH_4 conversion\ (\%) = \frac{mol\ of\ CH_4\ convered}{mols\ of\ CH_4\ in\ feed} \times 100$$

$$CO_2 conversion\ (\%) = \frac{mol\ of\ CO_2\ convered}{mols\ of\ CO_2\ in\ feed} \times 100$$

$$\frac{H_2}{CO} = \frac{mol\ of\ H_2\ produced}{mol\ of\ CO\ produced}$$

Results and Discussion

PN-Ceria (Fig. S1, ESI †) was synthesized through a two-step hydrothermal approach involving hydrothermal formation of nonporous nanorod precursor of $Ce(OH)_3/CeO_2$ at 100 ºC followed by dehydration and oxidation under hydrothermal conditions at 160 ºC.[33, 38, 39]

Characterization of Pt/nanoceria catalysts

Over the past few decades, it has been recognized that the nanoscaled and/or atomic characteristics of catalysts, such as surface structures, particle size and morphology, are critical to the catalytic activity and selectivity of nanocatalysts.[40, 41] However, an inherent technique problem of the nanocatalysts is lack of stability at the realistic operation conditions especially if the reaction temperature is very high and the reaction condition is very active. Generally, the rapid growth of supported active metal nanoparticles significantly decreases their activity for many industrial high temperature catalytic processes, such as reforming reactions and automobile exhaust treatments.[17, 21, 42] Meanwhile, the support itself has to be rigid enough at realistic conditions since the collapsed support may bury the nanocatalysts inside and block the accessibility of reactants towards the nanocatalysts.

The thermal stability of CeO_2 nanoparticles, *NR*-Ceria, ceria cube and *PN*-Ceria was evaluated at 600 ºC and 800 ºC for 4 hours under ambient conditions. CeO_2 nanoparticles were synthesized by thermal calcination of cerium nitrate in air at 500 ºC.[33] Nonporous ceria nanorods and nanocubes were prepared according to previous report.[35] TEM observation (Fig. S2, ESI †) and BET measurements (Fig. S3, ESI †) reveal that

PN-Ceria delivers the best thermal stability among all forms of nanocerias. The serious sintering of CeO_2 nanoparticles (Fig. S2a-2c, ESI †), ceria nanocubes (Fig. S2d-2f, ESI †) and *NR*-Ceria (Fig. S2g-2i, ESI †) was observed after 800 °C calcination for 4 h. It is also important to note that the porous feature of *PN*-Ceria (Fig. S2l, ESI †) was well preserved after 800 °C calcination for 4 h. Pt nanocatalysts loaded on *PN*-Ceria by wet impregnation method were used to study the thermal stability of catalysts for CRM.[15] The *NR*-Ceria was chosen as the comparative supports of Pt nanocatalysts due to its similar rod-like morphology and relative good thermal stability. The catalysts were denoted as Pt/*PN*-Ceria and Pt/*NR*-Ceria, respectively, when *PN*-Ceria and *NR*-Ceria were used as supports. The Pt content was 0.57 wt% for both catalysts, which was determined by ICP measurements.

Fig. 1 shows the bright field and dark field TEM images of Pt nanocatalysts on the *PN*-Ceria and *NR*-Ceria. For Pt/*PN*-Ceria, on obvious Pt particles could be observed (Fig. 1a and 1b), indicating the high dispersion of Pt on the support. In contrast, Pt nanoparticles were observed when the *NR*-Ceria was employed as the supports (Fig. 1c and 1d). The powder XRD patterns of the reduced catalysts exhibited in Fig. S4 (ESI †) show the characteristic peaks of fluorite-type oxide structure of CeO_2 (JCPDS No 75-0076) for both catalysts. No Pt phase was clearly observed for all samples, which could be attributed to the low Pt loading and highly dispersed Pt species on the supports that were able to be detected by XRD technique. The existence of Pt in the catalysts was further confirmed by the XPS spectra as shown in Fig. S5 (ESI †), in which the peak centered around 75.0 eV corresponds to Pt species.[9]

The BET surface area and pore volume of the freshly reduced catalysts were summarized in Table 1. Impregnation of Pt on the *PN*-Ceria support has a consequential impact on the BET specific surface area of the materials prepared. The surface area of the Pt/*PN*-Ceria catalysts was slightly reduced to 119.9 m^2/g, compared to 122.7 m^2/g of *PN*-Ceria. Pore volume of *PN*-Ceria was reduced from 0.378 cm^3 to 0.311 cm^3 for Pt/*PN*-Ceria. The slight decrease of specific surface area and pore volume after impregnation of Pt on the *PN*-Ceria supports might suggest the presence of Pt species at the end of pores or inside the pores of *PN*-Ceria. The surface area of Pt/*NR*-Ceria was 97.5 m^2/g, which was close to 98.3 m^2/g of *NR*-Ceria. Pt dispersion on supports is summarized in Table 1. When the Pt loading was equal in 0.57 wt%, a 41.4% Pt dispersion of Pt/*PN*-Ceria was much larger than that of Pt/*NR*-Ceria (25.6%), which might be attributed to the increased surface area and the rich surface defects of *PN*-Ceria support.

XPS analysis of the supports and Pt species on the supports

XPS analysis is performed to clarify the surface composition and chemical states for both the supports and Pt species on supports. The Ce 3d electron core level XPS spectra of CeO_2 and Pt/-Ceria

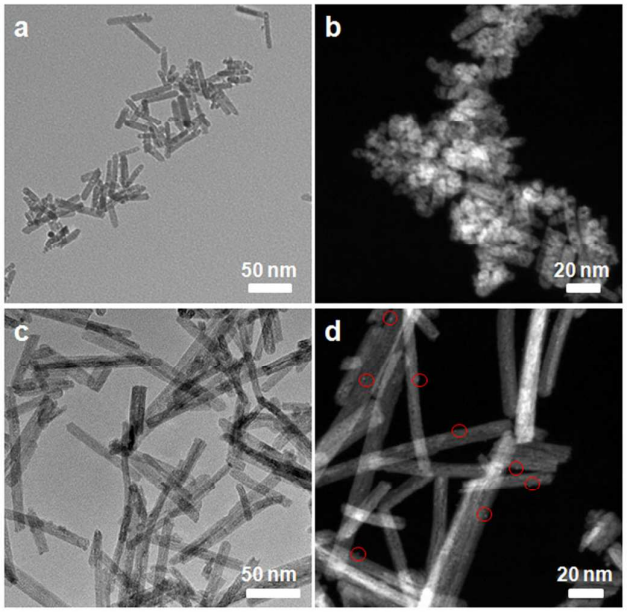

Fig. 1. (a) TEM images of the reduced Pt/*PN*-Ceria catalysts. (b) STEM images of the reduced Pt/*PN*-Ceria catalysts. (c) TEM images of the reduced Pt/*NR*-Ceria catalysts. (d) STEM images of the reduced Pt/*NR*-Ceria catalysts.

nanomaterials are shown in Fig. 2a. The Ce 3d XPS spectra are fitting according to eight peaks, denoted as two groups (*U*, *U'*, *U''*, *U'''* and *V*, *V'*, *V''*, *V'''*). The peaks of *U*, *U''*, *U'''* and *V*, *V''*, *V'''* refer to Ce(IV) $3d_{3/2}$ and $3d_{5/2}$,respectively, while both *U'* and *V'* stand for Ce(III) $3d_{3/2}$ and $3d_{5/2}$, respectively.[43] The surface Ce^{3+} concentrations of total Ce species on the *PN*-Ceria and *NR*-Ceria are 24.9 % and 18.4 %, while those of the Pt/*PN*-Ceria and Pt/*NR*-Ceria are 27.6 % and 19.6%, respectively. The presence of Ce^{3+} implies the defective structure of CeO_2 supports and the formation of oxygen vacancies. Oxygen vacancies can be produced via the transformation between Ce^{3+} and Ce^{4+}. Generally, the high concentration of oxygen vacancies is associated with high fraction of Ce^{3+}.[15, 44] After the deposition of Pt nanocatalysts on CeO_2 supports, the Ce^{3+} concentration also increases due to the interaction between metal and CeO_2 supports. The metal-support interaction effects change the surface electronic states, which makes the oxygen atom closed to Pt nanocatalysts and more easily to be reduced.[9] Therefore, part of high valence state of Ce^{4+} is converted to low valence state of Ce^{3+} and the number of oxygen vacancies is increased.

Redox Properties of Pt/CeO_2

Ceria exhibits structural defects of oxygen vacancies due to the reversibly Ce^{3+}/Ce^{4+} redox cycles. The oxygen vacancies are accepted as a common factor to directly affect catalytic activity of the materials. It has been widely reported that high reducibility and high oxygen storage capacity of the catalysts can effectively transfer oxygen to metal nanocatalysts, which can affect the catalytic activity of the catalysts and promote the removal of carbonaceous deposits on the catalytic sites in high

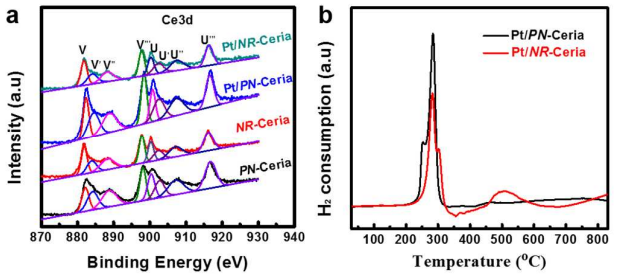

Fig. 2. XPS spectra of the Ce 3d core level regions for *PN*-Ceria and *NR*-CeO_2, Pt/*PN*-Ceria and Pt/*NR*-Ceria catalysts. (b) H_2-TPR profiles of Pt/*PN*-Ceria and Pt/*NR*-Ceria.

temperature reactions involving the carbon deposition [6, 42]. The H_2-TPR profiles represent the reducibility of the catalysts, which is associated with their ability to release O_2 from the catalysts through the reaction with H_2. Hence, H_2-TPR profile was used to evaluate the reducibility of *PN*-Ceria and the Pt/*PN*-Ceria catalysts. As a comparison, the reducibility of *NR*-Ceria and Pt/*NR*-Ceria was also evaluated side by side.

As shown in Fig. S6 (ESI †), H_2-TPR profiles of *PN*-Ceria and *NR*-Ceria indicated the amount of oxygen provided to CRM by *PN*-Ceria is much larger than that by *NR*-Ceria. H_2-TRP measurements were also performed on Pt/*PN*-Ceria and Pt/*NR*-Ceria catalysts (Fig. 2b). Obviously, both profiles exhibit a double strong reduction peaks at 220–350°C. The first peak at 281°C for Pt/*NR*-Ceria or at 250 °C for Pt/*PN*-Ceria was attributed to the reduction of Pt oxides. The second peak located at 302°C for Pt/*NR*-Ceria or at 281 °C for Pt/*PN*-Ceria corresponded to the reduction of surface ceria by the spillover of hydrogen generated from Pt.[45] The reduction peaks of Pt/*PN*-Ceria shifted to low temperatures compared to those of Pt/*NR*-Ceria, which can be attributed to the increased reduction extent of surface ceria of *PN*-Ceria.[46] The metal-support interaction effectively modifies the surface electronic states of catalysts, making the oxygen atom nearby Pt nanocatalysts more easily to be reduced. The intensity of the second reduction peaks for Pt/*PN*-Ceria catalysts was much stronger than that for Pt/*NR*-Ceria, indicating the stronger interaction between the platinum and *PN*-Ceria. The peak at 500 °C for Pt/*NR*-Ceria was attributed to the surface reduction process for ceria, which was not in close contact with Pt. The reduction peaks for *PN*-Ceria at high temperature were not observed, which could be attributed to the strong spillover of atomic hydrogen from Pt to *PN*-Ceria support.

Thermal stability of the Pt/CeO_2 catalysts

The thermal stability of Pt/CeO_2 catalysts was also evaluated by calcining the as-synthesized catalysts at 600 °C and 800 °C for 4 h under ambient conditions at a ramping rate of 1 ºC/min, respectively. The morphology evolution and surface area of Pt/CeO_2 catalysts were presented in Fig. 3 and Fig. 4. As shown in Fig. 3a and 3b, Pt/*PN*-CeO_2 catalysts exhibited a good thermal stability, and the porous morphology was well preserved at 600 °C and 800 °C, except the Pt/*PN*-CeO_2 catalysts were shortened at 800 °C (Fig.3b). From the dark field TEM images of Pt/*PN*-CeO_2 catalysts annealed at 600 °C and 800 °C in Fig. 3c and 3d, no obvious Pt particles could

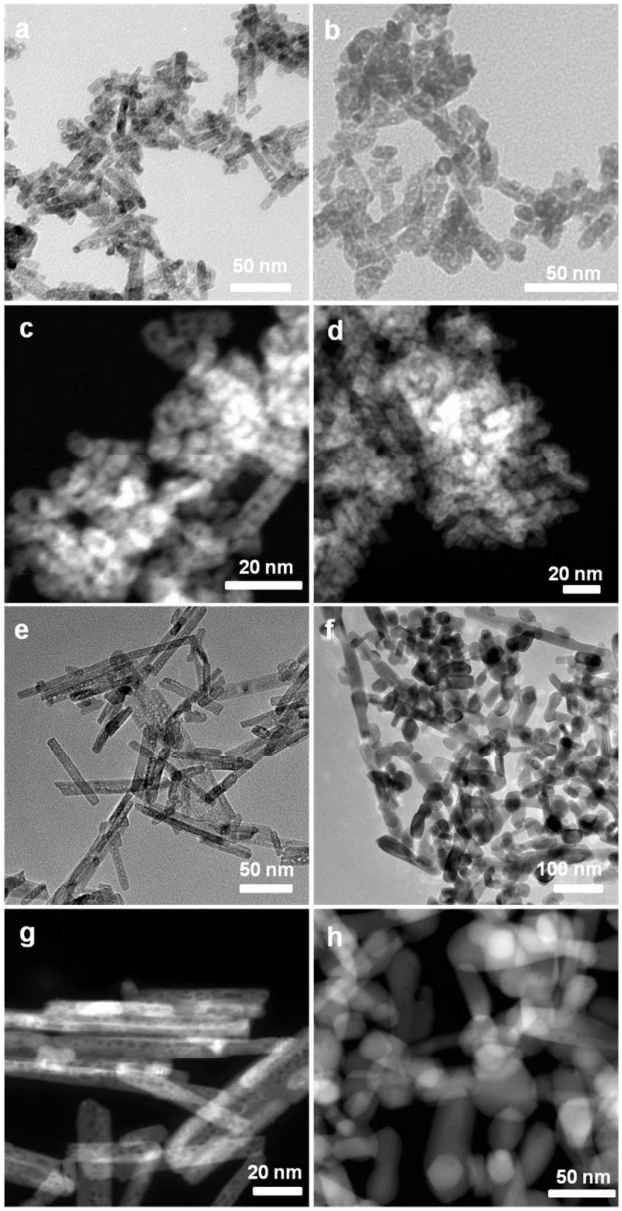

Fig. 3. (a) TEM characterization of Pt/*PN*-Ceria after calcination at 600 °C for 4h. (b) TEM characterization of Pt/*PN*-Ceria after calcination at 800 °C for 4h. (c) Dark field TEM characterization of Pt/*PN*-Ceria after calcination at 600 °C for 4h. (d) Dark field TEM characterization of Pt/*PN*-Ceria after calcination at 800 °C for 4h. (e) TEM characterization of Pt/ *NR*-Ceria after calcination at 600 °C for 4h. (f) TEM characterization of Pt/ *NR*-Ceria after calcination at 800 °C for 4h. (g) Dark field TEM characterization of Pt/*NR*-Ceria after calcination at 600 °C for 4h. (h) Dark field TEM characterization of Pt/*NR*-Ceria after calcination at 800 °C for 4h.

be observed. Fig. 3e and 3f showed the TEM images of the Pt/*NR*-Ceria after 600 °C and 800 °C calcination. After 600 °C calcination, the morphology of Pt/*NR*-Ceria was barely changed. In contrast, increasing the calcinations temperature to 800 °C led to collapsing and melting of the rod-like morphology of Pt/*NR*-Ceria into the spherical particles. The dark field TEM images of Pt/*NR*-CeO_2 catalysts annealed at 600 °C and 800 °C (Fig. 3g and 3h) further confirmed the morphological evolution. The Pt nanoparticles were

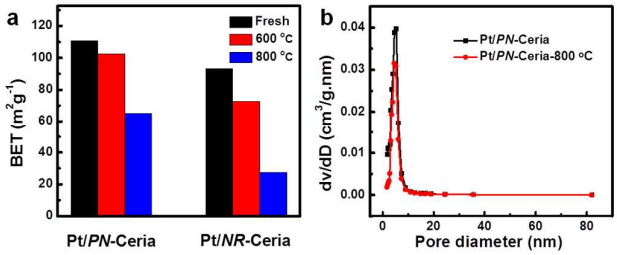

Fig. 4. The evolution of the surface areas of Pt/*PN*-Ceria and Pt/*NR*-Ceria treated at different calcination temperatures under ambient conditions.

also observed at 800 °C in Fig. 3h. The surface areas of Pt/*NR*-Ceria were significantly decreased to 72.5 and 27.4 m^2/g after 600 °C and 800 °C calcinations (Fig. 4a). In contrast, the surface areas of Pt/*PN*-Ceria after 600 °C and 800 °C calcination were 102.5 and 74.7 m^2/g, respectively. Meanwhile, the pore size distribution of the Pt/*PN*-CeO_2 catalysts after 800 °C calcination was similar to that of as-synthesized Pt/*PN*-CeO_2 catalysts (Fig. 4b). The morphology, surface areas and pore size distribution of Pt/CeO_2 catalysts confirmed that Pt/*PN*-CeO_2 catalysts exhibited better thermal stability.

Catalytic Performance

The catalytic activity of the catalysts was investigated for CRM reaction, which was carried out in a fixed catalytic bed with a flow mixture of CH_4, CO_2 and Ar within a temperature range of 500–800 °C. The GHSV was fixed at 30 000 mL/(g·h) for all reactions. Fig. 5a exhibits the CRM activity of Pt/*PN*-Ceria at different temperatures by plotting the conversion of CH_4 and CO_2 as a function of reaction temperatures. As temperature increases, the oxygen mobility is enhanced and lattice oxygen also can be activated to involve the reaction. Hence an increased conversion of CH_4 is expected at elevated temperature. As observed in Fig. 5a, the catalyst Pt/*PN*-Ceria showed the increased CH_4 conversion from 11.1% to 19.7%, 31.4%, 42.8%, 53.6%, 65.5% and 77.3%, corresponding to the temperatures of 500, 550, 600, 650, 700, 750 and 800°C, respectively. The CO_2 conversion (Fig. 5b) exhibited the similar behavior, which was increased with raising the reaction temperature. Of note, the ratio of H_2/CO in Fig. 5c was increased from 0.66 at 500 °C to 0.77 at 800°C, indicating that reversible water-gas shift reaction was suppressed at the high temperatures. Such a phenomenon has been generally observed for Pt-based catalysts for CRM.[23] Despite feeding of equimolar of methane and carbon dioxide for CRM reaction, CO_2 conversion was higher compared to conversion of CH_4 during the whole tested temperature range for all the catalysts. This could be attributed to co-occurrence of reverse water–gas shift reaction, consuming additional amounts of CO_2 (and H_2) to yield CO and water.[13, 23] This negatively influenced the H_2 yield and resulted in a H_2/CO ratio well below the thermodynamically predicted values of 1.0. Increasing reaction temperature led to an increased value for the ratio of H_2/CO due to the suppressed reversed water-gas shift reaction at high

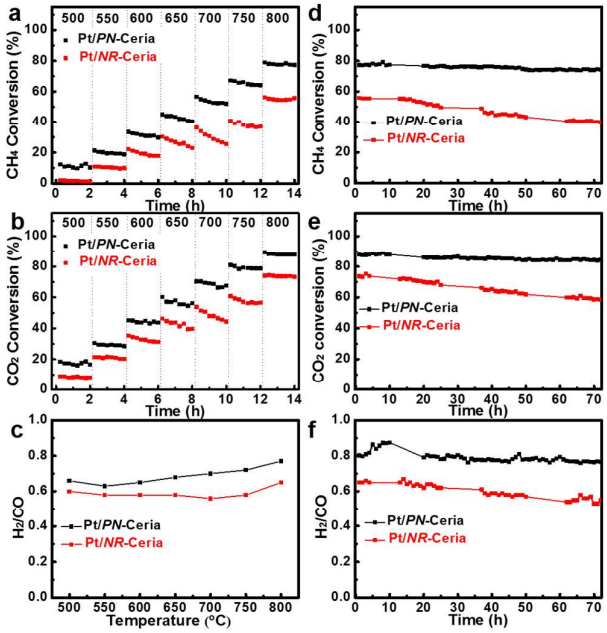

Fig. 5. Catalytic activity of Pt/*PN*-Ceria and Pt/*NR*-Ceria catalysts for the CRM as a function of temperature: (a) CH_4 conversion, (b) CO_2 conversion and (c) H_2/CO ratio. Catalytic stability of Pt/*PN*-Ceria and Pt/*NR*-Ceria catalysts for CRM at 800 °C as a function of time: (a) CH_4 conversion, (b) CO_2 conversion and (c) H_2/CO ratio.

temperature.[23]

As characterized by XPS and H_2-TPR, the support, *PN*-Ceria, displays a higher surface Ce^{3+} fraction, a high concentration of oxygen vacancies, a larger surface area and a better thermal stability, compared to the *NR*-Ceria as the support. Under the equal Pt loading, the Pt exhibited a much high dispersion on *PN*-Ceria than that on *NR*-Ceria (Table 1). Hence, the higher catalytic activity of Pt/*PN*-Ceria is expected, compared to that of Pt/*NR*-Ceria. The catalytic activity of Pt/*NR*-Ceria was also evaluated at the identical conditions. As shown in Fig. 5a, the conversions of CH_4 for Pt/*NR*- Ceria were 1.6%, 10.3%, 19.4%, 26.5%, 30.1%, 38.2% and 55.8% for 500, 550, 600, 650, 700, 750 and 800°C, respectively, which were much smaller than those of the Pt/*PN*-Ceria at the corresponded temperatures.

Stability Tests of Pt/CeO_2 Catalysts

TOS tests for the catalytic stability of both catalysts were performed at the same reaction conditions: CH_4:CO_2=1:1, 800 °C and a GHSV of 30 000 mL/(g·h) for 72 hours. Fig. 5d and 5f shows the CH_4 conversion, CO_2 conversion and the H_2/CO molar ratio in the product stream, respectively, as a function of the reaction time. As shown in Fig. 5d, the CH_4 conversion with time on stream over Pt/*PN*-Ceria was slightly dropped from 77.3 % to 74.2 % after 72 hours reaction. In contrast, the initial CH_4 conversion of 55.8 % for Pt/*NR*-Ceria was significantly decreased to 39.6 % at the end of 72 hour of TOS. The calculated CH_4 deactivation rate for Pt/*PN*-Ceria for a period of 72 hours was only 0.07 %/h, which was significantly lower than that (0.24 %/h) in a previous report for 1 % Pt/CeO_2 on stream at 800 °C for a duration of 60 hours.[47]

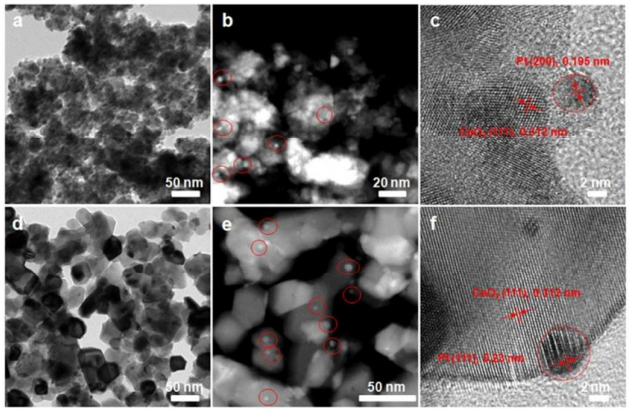

Fig. 6. TEM images of Pt/*PN*-Ceria and Pt/*NR*-Ceria catalysts for DCM at 800 °C for 72h. (a) TEM image of Pt/*PN*-Ceria catalysts, (b) Dark field TEM image of Pt/*PN*-Ceria catalysts, (c) HRTEM image of Pt/*PN*-Ceria, (d) TEM image of Pt/*NR*-Ceria, (e) Dark field TEM image of Pt/*NR*-Ceria, (f) HRTEM image of Pt/*NR*-Ceria.

The results illustrate the higher catalytic stability of the Pt catalysts on the *PN*-Ceria support towards CRM reaction at a high temperature of 800 °C. The same trend of CO_2 conversion was also observed as shown in Fig. 5e. Of note, H_2/CO molar ratio (Fig. 5f) with TOS for Pt/*PN*-Ceria showed a slight decrease, while a large decrease of H_2/CO ratio of Pt/*NR*-Ceria catalysts was observed from 0.65 to 0.55. Water drops were also observed at the downstream of the reactor when Pt/*NR*-Ceria was used. The results indicate that the reverse water-gas shift reaction is enhanced as time goes on for Pt/*NR*-Ceria.[23] Conclusively, the higher CH_4 and CO_2 conversions and the larger H_2/CO molar ratio of Pt/*PN*-Ceria catalysts at 800 °C for a long period than those of Pt/*NR*-Ceria catalysts with same Pt content illustrate the important role of supports on the catalytic performance for the loaded metal nanocatalysts.

Generally, stability of the catalysts can be reflected by three experimental phenomena: apparent thermal stability of supports and the catalysts, high metal dispersion and carbon deposition of the catalysts. Many factors including basicity of supports, concentrations of surface oxygen vacancies, oxygen storage capacity, interaction between support and metal and microstructures of the catalysts can significantly affect the observation in the morphological changes and catalytic activity of the catalysts. As revealed in Fig. S3 (ESI †), the *PN*-Ceria preserves a surface area (74.7 m^2/g) of as-synthesized *PN*-Ceria after calcination at 800 °C for 4 hours, which is much larger than that for *NR*-Ceria after the equal treatments. The remarkable thermal stability of *PN*-Ceria can provide more accessible active sites for catalytic reaction, leading to a stabilized catalytic activity. Meanwhile, Pt/*PN*-CeO_2 catalysts exhibit excellent thermal stability.

High metal dispersion is also critical for the catalytic stability since the deposited metal is the active component for CRM reaction process.[48, 49] We examined the metal dispersion of both catalysts after 72 hour reaction, as showed in Table 1. After 72 hours, the metal dispersion for the spent Pt/*PN*-Ceria was decreased and still maintained at 30.1%. However, the metal dispersion for Pt/*NR*-Ceria was seriously decreased from 25.6 % to 6.1 % under the identical conditions. Obviously, the Pt particles sintered seriously under catalytic reaction conditions for Pt/*NR*-Ceria and reduced the available amount of Pt catalytic sites for CRM reaction. The electron microscopy characterization on the spent catalysts after 72 hour reaction was presented in Fig. 6. The rod-like morphology of both catalysts was lost as evidenced in their TEM images. The bright field TEM (Fig. 6a) and dark field TEM (Fig. 6b) images indicated that the spent Pt/*PN*-Ceria catalysts exhibited the flower-like morphology composed of very small nanoparticles. Pt nanoparticles with a size of 3.8 nm ± 0.5 nm can be observed from the dark field TEM image (Fig. 6b) and high resolution TEM image (Fig. 6c). In contrast, the Pt/*NR*-Ceria catalysts showed a serious sintering after 72 h of reaction at 800°C. The rod-like morphology of the *NR*-Ceria was fully sintered into big spherical particles of ~ 33.7 nm (Fig. 6d). The dark field TEM image (Fig. 6e) and the HRTEM image (Fig. 6f) of the Pt/*NR*-Ceria catalysts showed the size of Pt nanoparticle was increased to 7.5 nm ± 0.7 nm. Both the melting of Pt/*NR*-Ceria and increased size of Pt nanoparticles will decrease the accessible reactive sites for the reactants.

Coking Characteristics of Pt/CeO_2 catalysts

Coke formation on the surface of catalysts operated at high temperature is a fatal problem for carbon dioxide reforming of methane, leading to a serious catalyst deactivation. The deactivation of catalysts can be explained by the blockage of metal sites, encapsulation of metal crystallites, and blockage of pores in the catalyst support.[50]

The temperature-programmed oxidation of the spent catalysts after 72-hour TOS was performed with the TGA-DSC techniques to evaluate coke formation for each catalyst, as quantificationally summarized in Table 1. The Pt/*PN*-Ceria catalysts showed a much lower coke formation (0.74 wt%, 0.10 mg coke · g_{cat}^{-1} · h^{-1} coke deposition rate) after CRM reaction at 800 °C for 72 h, which was much lower than that of Pt/*NR*-Ceria (2.44 wt%) with a carbon deposition rate of 0.34 mg coke · g_{cat}^{-1} · h^{-1}. The carbon deposition rate of our catalysts was much lower than the previous report with a coke deposition rate of 0.8-0.9 mg coke · g_{cat}^{-1} · h^{-1} over 1% Pt/CeO_2 during 60 h at 800 °C.[47] The very low carbon deposition on Pt/*PN*-Ceria catalysts can be explained by the unique structural features of the *PN*-Ceria and the strong interaction between Pt metal and *PN*-Ceria.

Firstly, *PN*-Ceria as support delivers a high concentration of oxygen vacancies associated with strong basicity. Carbon deposition during CRM can be originated from either CH_4 decomposition or CO disproportionation, which favorably happens on the acidic supports. In contrast, Lewis bases have a strong affinity for the chemisorption of CO_2 leaving oxygen on the catalyst surface, and the adsorbed oxygen reacts with carbonaceous deposits and promotes the ability of catalysts for anti-coke formation.[6, 49] Thereby, the basic support can effectively suppress the carbon deposition

Second factor is the strong interaction between Pt metal and *PN*-Ceria. It is well known that metal-support interaction is enhanced due to the oxygen-storage/transport characteristics of the *PN*-Ceria support or to the generation of active centers at

Table 1. Physicochemical Characteristics of Support and Pt/Ceria Catalysts.

Catalyst	BET $(m^2g^{-1})^a_{fresh}$	V_{pore} (cm^3)	Dispersion [b] $(\%)_{fresh}$	Dispersion [b] $(\%)_{spent}$	$Ce^{3+}/(Ce^{3+}+Ce^{4+})$ (%)	Carbon (wt.%)[c]
***PN*-Ceria**	**122.7**	**0.378**	**-**	**-**	**24.9**	**-**
Pt/*PN*-Ceria	**119.9**	**0.311**	**41.4**	**30.1**	**27.6**	**0.74**
***NR*-Ceria**	**98.3**	**0.185**	**-**	**-**	**18.4**	**-**
Pt/*NR*-Ceria	**97.5**	**0.184**	**25.6**	**6.1**	**19.6**	**2.44**

[a] BET results were determined by the ASAP 2020, Micromeritics Inc. [b] Determined from room temperature CO adsorption measurements, using the CHEMBET-3000. [c] The spent catalysts were firstly calcined at 800 °C in air for 30min for removal of carbon. Then, the Pt dispersion of spent catalysts was determined from room temperature CO adsorption measurements, using the CHEMBET-3000. [d] Coke deposition was quantified by thermogravimetry after 72 h on stream.

the interface between metal and support. Thus, the catalytic performance can be improved and the carbon deposition can be reduced.[18, 42, 44, 51] Compared to non-porous CeO_2 nanorods, Pt/*PN*-Ceria exhibits very large oxygen storage (~ 900 μmol O_2/g) and a higher concentration of oxygen vacancies and stronger basicity, ensuring the ability for anti-coke formation.

Conclusions

Porous nanorods of CeO_2 with a large surface area, a high concentration of oxygen vacancy, a high oxygen storage capacity and remarkable thermal stability exhibit the potentials as supports for metal nanocatalysts for high temperature catalysis. Compared with CeO_2 nanoparticles, CeO_2 cubes and nonporous nanorods of CeO_2, *PN*-Ceria preserved its morphological features at high temperature and maintained its large surface area for exposure of metallic reactive sites and approaching of reactants during catalytic reactions. High concentration of oxygen vacancies of *PN*-Ceria can benefit for stabilizing the small metal nanocatalysts at high temperature. The stronger basicity of *PN*-Ceria and highly dispersed Pt on *PN*-Ceria during catalytic process can effectively inhibit the carbon deposition, as low as 0.1 mg coke $\cdot$ $g_{cat}^{-1}\cdot$ h^{-1} for 72 hour TOS reaction. Catalytic activity of Pt/*PN*-Ceria catalysts in terms of methane conversion was only slightly decreased from 77.3 % to 74.2 % for a duration of 72 hours. As a result, the higher catalytic activity, better catalytic stability and higher coke resistance of Pt/*PN*-Ceria catalysts for the CRM reaction demonstrate the novel ceria nanostructure—porous nanorods of CeO_2, as a promising support for high temperature catalysis.

Acknowledgements

We acknowledge the financial support from a NSFC Grant 21201138. This work was also partially funded by the Ministry of Science and Technology of China through a 973-program under Grant 2012CB619401 and by the Fundamental Research Funds for the Central Universitiesunder Grant xjj2013102 and xjj2013043. Technical supports for TEM experiments from Frontier Institute of Science and Technology, Xi'an Jiaotong University, is also acknowledged.

Notes and references

1. Y. Lim, C. J. Lee, Y. S. Jeong, I. H. Song, C. J. Lee and C. Han, *Ind. Eng. Chem. Res.*, 2012, **51**, 4982-4989.
2. Z. Li, L. Mo, Y. Kathiraser and S. Kawi, *ACS Catal.*, 2014, **4**, 1526-1536.
3. M. C. J. Bradford and M. A. Vannice, *Cat. Rev. Sci. Eng.*, 1999, **41**, 1-42.
4. Y. H. Hu and E. Ruckenstein, *Cat. Rev. Sci. Eng.*, 2002, **44**, 423-453.
5. Y. Qu, A. M. Sutherland and T. Guo, *Energy Fuels*, 2008, **22**, 2183-2187.
6. A. G. Bhavani, W. Y. Kim and J. S. Lee, *ACS Catal.*, 2013, **3**, 1537-1544.
7. N. Wang, W. Chu, T. Zhang and X. S. Zhao, *Int. J. Hydrogen Energy*, 2012, **37**, 19-30.
8. I. Luisetto, S. Tuti and E. Di Bartolomeo, *Int. J. Hydrogen Energy*, 2012, **37**, 15992-15999.
9. W. Tang, Z. Hu, M. Wang, G. D. Stucky, H. Metiu and E. W. McFarland, *J. Catal.*, 2010, **273**, 125-137.
10. S. B. Wang and G. Q. M. Lu, *Energy Fuels*, 1996, **10**, 896-904.
11. G. C. d. Araujo, S. M. d. Lima, J. M. Assaf, M. A. Peña, J. L. G. Fierro and M. do Carmo Rangel, *Catal. Today*, 2008, **133-135**, 129-135.
12. E. Ruckenstein and H. Y. Wang, *J. Catal.*, 2002, **205**, 289-293.
13. X. Xie, T. Otremba, P. Littlewood, R. Schomäcker and A. Thomas, *ACS Catal.*, 2013, **3**, 224-229.
14. V. M. Gonzalez-Delacruz, F. Ternero, R. Pereñíguez, A. Caballero and J. P. Holgado, *Appl. Catal., A*, 2010, **384**, 1-9.
15. S. Damyanova, B. Pawelec, K. Arishtirova, M. V. M. Huerta and J. L. G. Fierro, *Appl. Catal., B*, 2009, **89**, 149-159.
16. A. M. d. Silva, K. R. d. Souza, G. Jacobs, U. M. Graham, B. H. Davis, L. V. Mattos and F. B. N. , *Appl. Catal. B*, 2011, **102**, 94-109.
17. J. Lu, B. Fu, M. C. Kung, G. Xiao, J. W. Elam, H. H. Kung and P. C. Stair, *Science*, 2012, **335**, 1205-1208.
18. T. Odedairo, J. Chen and Z. Zhu, *Catal. Commun.*, 2013, **31**, 25-31.
19. M. Ocsachoque, F. Pompeo and G. Gonzalez, *Catal. Today*, 2011, **172**, 226-231.
20. M. Cai, J. Wen, W. Chu, X. Cheng and Z. Li, *J. Nat. Gas Chem.*, 2011, **20**, 318-324.
21. S. Zhang, S. Muratsugu, N. Ishiguro and M. Tada, *ACS Catal.*, 2013, **3**, 1855-1864.
22. C. Aydin, J. Lu, N. D. Browning and B. C. Gates, *Angew. Chem. Int. Ed. Engl.*, 2012, **51**, 1-7.
23. N. Wang, K. Shen, L. Huang, X. Yu, W. Qian and W. Chu, *ACS Catal.*, 2013, **3**, 1638-1651.
24. J. A. Farmer and C. T. Campbell, *Science*, 2010, **329**, 933-936.

25. L. Xu, H. Song and L. Chou, *ACS Catal.*, 2012, **2**, 1331-1342.
26. Y. Qu, A. M. Sutherland, J. Lien, G. D. Suarez and T. Guo, *J. Phys. Chem. Lett.*, 2010, **1**, 254-259.
27. A. Cao and G. Veser, *Nat. Mater.*, 2010, **9**, 75-81.
28. D. Liu, X. Y. Quek, W. N. E. Cheo, R. Lau, A. Borgna and Y. Yang, *J. Catal.*, 2009, **266**, 380-390.
29. Y.-H. Wang, H. M. Liu and B. Q. Xu, *J. Mol. Catal. A: Chem.*, 2009, **299**, 44-52.
30. Y. Li, G. Lu and J. Ma, *RSC Advances*, 2014, **4**, 17420-17428.
31. C. Chen, C. Nan, D. Wang, Q. Su, H. Duan, X. Liu, L. Zhang, D. Chu, W. Song, Q. Peng and Y. Li, *Angew. Chem. Int. Ed. Engl.*, 2011, **50**, 3725-3729.
32. M. S. Aw, I. G. Osojnik Črnivec, P. Djinović and A. Pintar, *Int. J. Hydrogen Energy*, 2014, **39**, 12636-12647.
33. J. Li, Z. Zhang, Z. Tian, X. Zhou, Z. Zheng, Y. Ma and Y. Qu, *J. Mater. Chem. A*, 2014, **2**, 16459-16466.
34. L. Feng, D. T. Hoang, C.-K. Tsung, W. Huang, S. H.-Y. Lo, J. B. Wood, H. Wang, J. Tang and P. Yang, *Nano Research*, 2010, **4**, 61-71.
35. H. Mai, L. Sun, Y. Zhang, R. Si, W. Feng, H. Zhang, H. Liu and C. Yan, *J. Phys. Chem. B*, 2005, **109**, 24380-24385.
36. W. Gao, Z. Zhang, J. Li, Y. Ma and Y. Qu, *Nanoscale*, 2015, **7**, 11686-11691.
37. A. Djaidja, S. Libs, A. Kiennemann and A. Barama, *Catal. Today*, 2006, **113**, 194-200.
38. Z. Tian, J. Li, Z. Zhang, W. Gao, X. Zhou and Y. Qu, *Biomaterials*, 2015, **59**, 116-124.
39. S. Zhang, J. Li, W. Gao and Y. Qu, *Nanoscale* 2015, **7**, 3016-3021.
40. Y. Li, Q. Liu and W. Shen, *J. Chem. Soc., Dalton Trans.*, 2011, **40**, 5811-5826.
41. A. Z. Moshfegh, *J. Phys. D: Appl. Phys.*, 2009, **42**, 233001.
42. V. Sadykov, V. Muzykantov, A. Bobin, N. Mezentseva, G. Alikina, N. Sazonova, E. Sadovskaya, L. Gubanova, A. Lukashevich and C. Mirodatos, *Catal. Today*, 2010, **157**, 55-60.
43. E. Paparazzo, *Appl. Catal., B*, 2011, **105**.
44. X. Du, D. Zhang, L. Shi, R. Gao and J. Zhang, *J. Phys. Chem. C*, 2012, **116**, 10009-10016.
45. K. R. Hwang, S. K. Ihm and J. S. Park, *Fuel Process Technol.*, 2010, **91**, 729–736.
46. S. Ricote, M. Milling, G. Jacobs, Y. Y. Ji, P. M. Patterson and B. H. Davis, *Appl. Catal., A*, 2006, **303**, 35–47.
47. M. M. V. M. Souzaa and M. Schmal, *Catal. Lett.*, 2003, **91**, 11-17.
48. S. Li and J. Gong, *Chem. Soc. Rev.*, 2014, **43**, 7245-7256.
49. J. Zhu, X. Peng, L. Yao, X. Deng, H. Dong, D. Tong and C. Hu, *Int. J. Hydrogen Energy*, 2013, **38**, 117-126.
50. M. M. Barroso-Quiroga and A. E. Castro-Luna, *Int. J. Hydrogen Energy*, 2010, **35**, 6052-6056.
51. V. A. Sadykov, E. L. Gubanova, N. N. Sazonova, S. A. Pokrovskaya, N. A. Chumakova, N. V. Mezentseva, A. S. Bobin, R. V. Gulyaev, A. V. Ishchenko, T. A. Krieger and C. Mirodatos, *Catal. Today*, 2011, **171**, 140-149.

Pt/Porous Nanorods of Ceria as Efficient High Temperature Catalysts with Remarkable Catalytic Stability for Carbon Dioxide Reforming of Methane

Zhiyun Zhang [a], Jing Li [a], Wei Gao [a], Yuanyuan Ma [a] *, Yongquan Qu [ab]*

[a] *Center for Applied Chemical Research, Frontier Institute of Science and Technology, and State key Laboratory for Mechanical Behavior of Materials, Xi'an Jiaotong University, Xi'an, China 710049*

[b] *MOE Key Laboratory for Nonequilibrium Synthesis and Modulation of Condensed Matter, Xi'an Jiaotong University, Xi'an, China 710049.*

E-mail: yongquan@mail.xjtu.edu.cn; yyma@mail.xjtu.edu.cn

Porous nanorods of CeO_2 (*PN*-Ceria) with a large surface area, a high oxygen storage capacity and remarkable thermal stability exhibit potentials as supports for metal catalysts. Combining their intrinsic physiochemical properties, the high catalytic activity, long-term stability and effectively suppressed carbon deposition of Pt/*PN*-Ceria catalysts have been demonstrated by carbon dioxide reforming of methane reaction at 800 ºC.